Rock and Soil Mechanics

Volume 43 | Issue 1 Article 6

3-23-2022

Stability analysis and visualization of rock slope blocks based on the coordinate projection method

Bing-li GAO
College of Architecture and Civil Engineering, Xi'an University of Science and Technology, Xi'an, Shaanxi 710054, China

Duo LI
College of Architecture and Civil Engineering, Xi'an University of Science and Technology, Xi'an, Shaanxi 710054, China

Lang LI
China Jikan Research Institute of Engineering Investigations and Design, Co. Ltd, Xi'an, Shaanxi 710043, China

Li-cheng CHEN
Suzhou FaceAll Technology Co. Ltd., Suzhou, Jiangsu 215124, China

See next page for additional authors

Custom Citation

GAO Bing-li, LI Duo, LI Lang, CHEN Li-cheng, YANG Zhi-fa, . Stability analysis and visualization of rock slope blocks based on the coordinate projection method[J]. Rock and Soil Mechanics, 2022, 43(1): 181-194.

Stability analysis and visualization of rock slope blocks based on the coordinate projection method

Authors

Bing-li GAO, Duo LI, Lang LI, Li-cheng CHEN, and Zhi-fa YANG

Rock and Soil Mechanics 2022 43(1): 181−194 ISSN 1000−7598
https: //doi.org/10.16285/j.rsm.2021.6059 rocksoilmech.researchcommons.org/journal

Stability analysis and visualization of rock slope blocks based on the coordinate projection method

GAO Bing-li[1], LI Duo[1], LI Lang[2], CHEN Li-cheng[3], YANG Zhi-fa[4]

1. College of Architecture and Civil Engineering, Xi'an University of Science and Technology, Xi'an, Shaanxi 710054, China
2. China Jikan Research Institute of Engineering Investigations and Design, Co. Ltd, Xi'an, Shaanxi 710043, China
3. Suzhou FaceAll Technology Co. Ltd., Suzhou, Jiangsu 215124, China
4. Institute of Geology and Geophysics, Chinese Academy of Sciences, Beijing 100029, China

Abstract: Block collapse or sliding is one of the main failure modes of rock slope engineering. Namely, block stability analysis plays a key role in rock slope engineering. Taking the Shenxianju rock slope in Xianju County, Zhejiang Province as the research background, this paper mainly conducts the stability analysis and visualization of rock blocks. A new method for fitting structural planes and free faces is proposed based on the linear regression method and the non-uniform rational B-spline method. Then, based on the coordinate projection method, the method for calculating the stability coefficients of the single sliding surface and double sliding surface blocks is proposed. Finally, the unmanned aerial vehicle (UAV) measurement technology combined with the coordinate projection method is used to develop a CPG program using MATLAB, which can be adopted in the stability analysis of planar polyhedron blocks and curved blocks in rock slope engineering. This program enables the spatial representation and visualization of structural planes, free faces and unstable blocks. Engineering practice shows that the new proposed method is effectively applicable to engineering geological disasters, such as rockfall and collapse. The results of the program calculation are basically consistent with those of the coordinate projection block theory, demonstrating that this method is reliable and the developed CPG program is feasible. This method is of vital significance in practical engineering since it can greatly improve the efficiency of block stability analysis.

Keywords: rock slope; coordinate projection; structural plane; block stability; visualization

1 Introduction

Rock masses consist of structural planes and structural blocks. The structural blocks are rock units cut by the structural planes, so the stability of rock masses is determined by the stability of structural blocks, and the stability of structural blocks is highly dependent on the characteristics, strength, their combinations with each other, and interaction force of structural planes. A large number of engineering practices show that the stability of engineering rock masses[1] is controlled by the structural plane. When subjected to external loads, the structural plane is deformed and damaged, which directly affects the deformation and failure of rock masses cut by structural planes and free faces. In rock slope engineering, rock mass failures mainly appear as block instabilities, and the block stability is closely related to the classification and support design of the surrounding rock. Therefore, the study of the block stability is closely associated with engineering practices. For the design and construction of rock slope engineering, the block stability analysis constitutes a vitally important part in the study of the overall stability of rock slope engineering.

Many methods, such as the numerical method, the stereographic projection mapping method, and the coordinate projection method, can be applied in the block geometric condition and stability analyses[2]. Goodman et al.[3] systematically proposed the block theory, which can be used in the block identification and stability problems induced by the combinations of spatially arbitrary structural planes and free faces. Sun et al.[4] adopted the stereographic projection for the block identification and stability analysis in rock engineering. Shi[5] studied the combination of structural planes and excavation free faces to analyze the blocks that may be generated after the excavation of slopes and tunnels by the stereographic projection and vector operation methods. Lin et al.[6] further investigated the identification of blocks with complex geometries in the three-dimensional (3D) space based on the topology principle. For the difficulty of evaluating the risk of block failures in underground caverns under complex geological conditions, Du et al.[7] proposed a block instability risk evaluation method based on the mutation theory. With the development of computer technology, Yossef et al.[8] developed a search program for key

Received: 12 July 2021 Revised: 12 September 2021
This work was supported by the National Key Research and Development Program of China (2019YFC1509703) and the Key Research and Development Program of Shaanxi Province (2021ZDLGY07−08).
First author: GAO Bing-li, female, born in 1980, PhD, Associate Professor, research interests: engineering geology and disaster prevention and mitigation. E-mail: gbl8001@126.com

blocks in the excavation process of underground engineering based on the block theory. According to the beam theory and block theory, Chen et al.[9] established a rock beam−block mechanical model to reveal the failure mode of the direct roof in the weak layer. Jiang et al.[10] proposed to optimize the probability distribution of structural plane geometry and shear strength parameters based on the Bayesian update method. Moreover, considering the uncertainty of structural plane geometry and shear strength parameters, the reliability analysis of jointed rock slopes was carried out by the non-intrusive stochastic finite element method. Combining the effects of the anisotropy of the structural plane roughness and shear strength on the deformation and stability of rock masses, Ding et al.[11] studied the 3D structural plane evaluation method and obtained the 3D structural plane shear strength calculation formulae.

Liu et al.[12] proposed a new semi-deterministic block theory (NSDBT), taking the dimensions, spatial location, and orientation of discontinuities into account to obtain the location, volume, and sliding force of critical rock blocks to provide quantitative guidance for the support design. Guo et al.[13] developed a method for automatically extracting the structural plane information of rock masses based on 3D point clouds, which can be applied in the deformation analysis and stability evaluation of rock masses. Francioni et al. [14] used the remote sensing technique to obtain rock mass characterization and discussed whether the resultant data could be used in the rock mass stability analysis. Jia et al.[15] used small unmanned aerial vehicles (UAVs) to perform 3D reconstruction of the target object based on patch-based multiview stereo (PMVS) and structure from motion (SFM) algorithms, and Wu[16] further developed the software for the block stability visualization and analysis. Using the limit equilibrium method and the strength reduction method, Zhou et al.[17] calculated the safety factors of some exposed blocks in the underground plant of a mega hydropower station under construction, and thus proposed a simple graphical method to evaluate the block stability based on the geometric and mechanical parameters and calculation results.

Wang et al.[18] proposed a block identification method based on the UAV photogrammetry and further computerized it, i.e., the real-time block monitoring by the SFM method and the DEM model of rock masses established through the 3D modeling software Photoscan. Albarelli et al.[19] proposed a method of acquiring data using UAV and obtaining accurate high-resolution geometric information of rock masses from 3D point clouds to evaluate the local rock avalanche stability. Zhang et al.[20] introduced the basic steps of the general block (GB) analysis method and examined the block stability of the Three Gorges underground hydropower station.

Jin et al.[21] adopted small single-lens UAVs to perform low-altitude photogrammetry on slopes to obtain high-precision digital elevation models (DEM), which could be transformed into 3D FLAC models by some software, such as Surfer and Rhino. This can rapidly establish 3D numerical models from UAV measurements. Wang et al.[22] proposed a rock block identification method based on the aerial photogrammetry and applied it to a rock wall after computerization, and the real 3D rock model was established by the improved bundle adjustment method. Liu et al.[23] proposed an integrated system combining the 3D-discontinuous deformation analysis (3D-DDA) method and the UAV photogrammetry as a tool for analyzing the stability of rock slope blocks. The system includes an UAV-LS module, a modeling module, a block generation module, and a 3D-DDA calculation module. Wang et al.[24] proposed the concept of a key block instability characterization coefficient to control slope stability. The coefficient can be applied in the key block search module of the geotechnical structures and the 3D Model Analysis (Geo SMA-3D) program to identify and visualize key blocks.

Yang[25] proposed the coordinate projection method by combining the stereographic projection and the orthographic projection, and applied it in the block stability analysis of rock engineering. Some achievements have been made through the research. Due to the function of integrating the complex information of structural planes and free faces, the coordinate projection method can easily express the geometric conditions of blocks, namely, it can well solve the problem of describing the geometric conditions of blocks with complex shapes and multi-blocks. Hence, this paper further examines the block stability based on the coordinate projection method.

Since the coordinate projection mapping of blocks, especially multi-blocks, is more complicated and the mapping efficiency is at a low level, the authors computerized it and developed the CPH program[26−27], but the program can be only used in the calculation of plane tetrahedral blocks, excluding the plane polyhedral blocks and curved surface blocks in rock slope engineering. Therefore, in this paper, the block stability analysis based on the coordinate projection principle will be conducted. Meanwhile, combined with the UAV technology, the CPG program applicable to the coordinate projection method will be developed for the stability analysis of plane polyhedral blocks and curved surface blocks in rock slope engineering. With

the CPG program, a 3D slope model can be constructed to realize the stability analysis and visualization of rock slope blocks.

2 Stability analysis of rocky slope blocks

2.1 Coordinate projection method

The coordinate projection method[25, 28−30] is a mapping method that combines the orthographic projection with stereographic projection in the rectangular coordinate system to analyze the geometric conditions and stability of blocks cut by structural planes and free faces in rock engineering. Its theoretical basis consists of the engineering geomechanics of rock masses, descriptive geometry and stereographic projection.

When analyzing the block stability using the coordinate projection method, the quantitative analysis of the blocks cut by structural planes and free faces is firstly carried out, i.e., the shape, location, volume, and boundary surface area of blocks are determined; then, the stability coefficient of blocks needs to be solved by the stability analysis method to identify the potential unstable blocks, thereby evaluating the overall stability of the rock engineering.

2.2 Block geometry identification

To analyze the stability of rocky slope blocks, it is necessary to find the blocks exposed on the free faces of the rocky slope and take the location, shape, and stability of these blocks as the research focus. Closed blocks can be generated only if multiple groups of structural planes and free faces form a closed space, and the premise of forming the closed blocks cut by the structural planes is that the exposed traces of the structural planes on the free faces are closed loops.

2.2.1 Determination of structural planes and free faces

In space, structural planes are approximately planar, while free faces are mostly curved. In this paper, the equation of the structural plane is determined by the linear regression fitting method, in which as many points not on the same line of the structural plane are selected as possible, and the linear regression equation is fitted using the spatial coordinates of these points to obtain the equation of the structural plane. For the determination of free faces, the non-uniform rational B-spline (NURBS) method[31−32] is used to construct the equation of the free face using the point cloud data on the free face of rock masses.

2.2.1.1 Determination method of structural planes

The structural plane is spatially approximated as a plane. The linear regression fitting method is used to fit the equation of the planar structural plane by selecting as many points on the structural plane traces as possible, and the equation is

$$z_i = \theta_0 + \theta_1 x_i + \theta_2 y_i + \mu_i, i = 1, 2, \cdots n \tag{1}$$

where θ_0, θ_1, and θ_2 are partial regression coefficients; μ_i is the random error; n is the number of selected points on the structural plane traces; and (x_i, y_i, z_i) is the coordinate of the structural plane.

The least square method is adopted to calculate the partial regression coefficients. Based on a set of coordinate data on the structural plane (x_i, y_i, z_i), a regression model is established, i.e., the equation of the structural plane $\hat{z}_i$ is as follows:

$$\hat{z}_i = \hat{\theta}_0 + \hat{\theta}_1 x_i + \hat{\theta}_2 y_i + e_i \tag{2}$$

where $\hat{\theta}_0$, $\hat{\theta}_1$, and $\hat{\theta}_2$ are the parameter estimates; and e_i is the random error.

To achieve the best fit, the mean square error $Q(\hat{\theta}_0, \hat{\theta}_1, \hat{\theta}_2)$, i.e.,

$$Q\left(\hat{\theta}_0, \hat{\theta}_1, \hat{\theta}_2\right) = \sum_{i=1}^{n} (z_i - \hat{z}_i)^2 = \sum_{i=1}^{n} (z_i - \hat{\theta}_0 - \hat{\theta}_1 x_i - \hat{\theta}_2 y_i)^2 \tag{3}$$

Eq.(3) reaches the minimum value.

According to the necessary conditions for the existence of extreme values:

$$\left.\begin{aligned} \frac{\partial Q(\hat{\theta}_0, \hat{\theta}_1, \hat{\theta}_2)}{\partial \hat{\theta}_0} &= -2\sum_{i=1}^{n} (z_i - \hat{\theta}_0 - \hat{\theta}_1 x_i - \hat{\theta}_2 y_i) = 0 \\ \frac{\partial Q(\hat{\theta}_0, \hat{\theta}_1, \hat{\theta}_2)}{\partial \hat{\theta}_1} &= -2\sum_{i=1}^{n} (z_i - \hat{\theta}_0 - \hat{\theta}_1 x_i - \hat{\theta}_2 y_i) x_i = 0 \\ \frac{\partial Q(\hat{\theta}_0, \hat{\theta}_1, \hat{\theta}_2)}{\partial \hat{\theta}_2} &= -2\sum_{i=1}^{n} (z_i - \hat{\theta}_0 - \hat{\theta}_1 x_i - \hat{\theta}_2 y_i) y_i = 0 \end{aligned}\right\} \tag{4}$$

The regular system of equations can be obtained:

$$\left.\begin{aligned} \sum_{i=1}^{n} Q(\hat{\theta}_0, \hat{\theta}_1, \hat{\theta}_2) &= 0 \\ \sum_{i=1}^{n} Q(\hat{\theta}_0, \hat{\theta}_1, \hat{\theta}_2) x_i &= 0 \\ \sum_{i=1}^{n} Q(\hat{\theta}_0, \hat{\theta}_1, \hat{\theta}_2) y_i &= 0 \end{aligned}\right\} \tag{5}$$

If there is no linear relation between x_i and y_i, $\hat{\theta}_0$, $\hat{\theta}_1$, $\hat{\theta}_2$ can be obtained by solving Eq.(5):

$$\left.\begin{aligned} \hat{\theta}_0 &= \bar{z} - \hat{\theta}_1 \bar{x} - \hat{\theta}_2 \bar{y} \\ \hat{\theta}_1 &= \frac{(\sum Z_i X_i)(\sum Y_i^2) - (\sum Z_i Y_i)(\sum X_i Y_i)}{(\sum X_i^2)(\sum Y_i^2) - (\sum X_i Y_i)^2} \\ \hat{\theta}_2 &= \frac{(\sum Z_i Y_i)(\sum X_i^2) - (\sum Z_i X_i)(\sum X_i Y_i)}{(\sum X_i^2)(\sum Y_i^2) - (\sum X_i Y_i)^2} \end{aligned}\right\} \tag{6}$$

where $X_i = x_i - \bar{x}$; $Y_i = y_i - \bar{y}$; $Z_i = z_i - \bar{z}$; $\bar{x} = \frac{1}{n}\sum x_i$; $\bar{y} = \frac{1}{n}\sum y_i$; and $\bar{z} = \frac{1}{n}\sum z_i$, $i = 1, 2, ...n$.

The equation of the structural plane $\hat{z}_i$ can thus be obtained, according to which the normal vector $(-\theta_1,-\theta_2,1)$ of the structural plane can also be obtained. The dip direction α and angle β of the structural plane of the rock mass can be acquired by the following equation:

$$\beta=\arccos\left(\frac{1}{\sqrt{\theta_1^2+\theta_2^2+1}}\right) \tag{7}$$

$$\left.\begin{aligned}&\alpha=\arcsin(-\theta_1/\sin\beta),\ -\theta_1\geqslant 0,-\theta_2\geqslant 0\\&\alpha=360°-\arcsin(\theta_1/\sin\beta),\ -\theta_1<0,-\theta_2>0\\&\alpha=180°-\arcsin(-\theta_1/\sin\beta),\ -\theta_1<0,-\theta_2<0\\&\alpha=180°+\arcsin(\theta_1/\sin\beta),\ -\theta_1>0,-\theta_2<0\end{aligned}\right\} \tag{8}$$

After determining the occurrence information of the structural plane, the extended range of the structural plane also needs to be determined. Xu et al.[33] pointed that the joints in crystalline rocks are approximately circular and those in sedimentary rocks are approximately rectangular in morphology. To simplify the calculation, the structural plane is assumed to be disc-shaped with the distance between the two farthest points on the trace as its diameter, and its spatial extension direction can be determined by the occurrence information.

2.2.1.2 Determination method of free faces

To visualize the free face, NURBS modeling, i.e., the non-uniform rational B-spline method, was adopted to construct the equation of the free face.

Let $\boldsymbol{U}=\{u_0,\cdots,u_{m+k}\}$, a monotonically non-decreasing sequence of real numbers, where u_i is the node; the number of spline basis functions i=0, 1, … , m; $\boldsymbol{U}$ is the node vector; and $N_{i,k}(u)$ is the ith k-order (k is the order of spline basis functions) B-spline basis function, which can be defined as

$$N_{i,0}=\begin{cases}1, & if\ u_i\leqslant u<u_{i+1}\\0, & else\end{cases} \tag{9}$$

$$N_{i,k}(u)=\frac{u-u_i}{u_{i+k}-u_i}N_{i,k-1}(u)+\frac{u_{i+k+1}-u}{u_{i+k+1}-u_{i+1}}N_{i+1,k-1}(u) \tag{10}$$

The NURBS curve shown in Fig. 1 can be expressed as

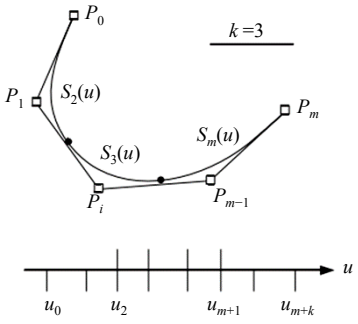

Fig. 1 NURBS curves

$$P(u)=\frac{\sum_{i=1}^{n}\omega_i p_i N_{i,k}(u)}{\sum_{j=0}^{n}\omega_j N_{j,k}(u)} \tag{11}$$

Let $R_{i,k}(u)=\dfrac{\omega_i N_{i,k}(u)}{\sum_{j=0}^{n}\omega_j N_{j,k}(u)}$, and then

$$P(u)=\sum_{i=0}^{n}P_i R_{i,k}(u) \tag{12}$$

where P_i is the control point; ω_i is the weight factor corresponding to P_i; and $P(u)$ is the position vector on the curve.

For a given NURBS curved surface, it can be regarded as a control network consisting of (m+1) × (n+1) control vertices by multiple NURBS curves in the $\boldsymbol{u}$ and $\boldsymbol{v}$ directions. An example of a bidirectional cubic NURBS curved surface is shown in Fig. 2, and the expression for a NURBS curved surface with $k \times l$ order is expressed as

$$\boldsymbol{s}(u,v)=\frac{\sum_{i=0}^{m}\sum_{j=0}^{n}N_{i,k}(u)N_{j,l}(v)\boldsymbol{p}_{i,j}\omega_{i,j}}{\sum_{i=0}^{m}\sum_{j=0}^{n}N_{i,k}(u)N_{j,l}(v)\omega_{i,j}} \tag{13}$$

where control vertex $\boldsymbol{p}_{i,j}$ (i=0, 1, … , m; j=0, 1, … , n) form a control grid in a topologically rectangular array; $\omega_{i,j}$ is the weight factors of control vertex $\boldsymbol{p}_{i,j}$; $N_{i,k}(u)$(i=0, 1,…, m) is the k-order non-rational B-sample basis functions on the node vector $\boldsymbol{U}$; and $N_{j,l}(v)$(j=0, 1,…, n) is l-order non-rational B-spline basis function on the node vector $\boldsymbol{V}$. $\boldsymbol{U}$ and $\boldsymbol{V}$ are derived from the node vectors in $\boldsymbol{u}$- and $\boldsymbol{v}$-directions:

$$\boldsymbol{U}=\left[u_0,\cdots,u_{m+k+1}\right] \tag{14}$$

$$\boldsymbol{V}=\left[v_0,\cdots,v_{m+k+1}\right] \tag{15}$$

According to the de Boer recurrence formula, where u_i and v_i are node values.

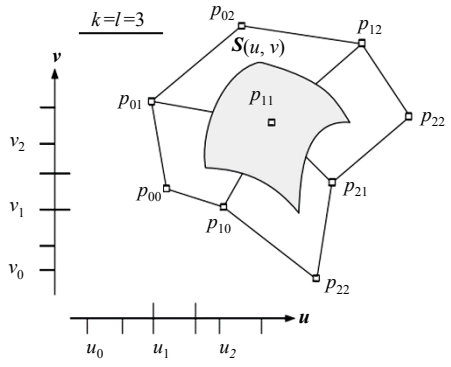

Fig. 2 NURBS curved surface (bidirectional and cubic)

For the convenience of programming, the NURBS curved surface is represented in homogeneous coordinates by the following expressions:

$$\boldsymbol{p}_{i,j}=\left(x_{i,j},\ y_{i,j},\ z_{i,j}\right) \tag{16}$$

$$\boldsymbol{S}(u,v)=\sum_{i=0}^{m}\sum_{j=0}^{n}N_{i,k}(u)N_{j,l}(v)\boldsymbol{P}_{i,j} \tag{17}$$

where $\boldsymbol{P}_{i,j}=[\omega_{i,j}\boldsymbol{p}_{i,j},\omega_{i,j}]$ is the weighted control vertex or the homogeneous coordinate of the control vertex $\boldsymbol{p}_{i,j}$; so $\boldsymbol{s}(u,v)=H(\boldsymbol{S}(u,v))$; H is the perspective projection of the projection center at the origin; and the weight factor $\omega_{i,j}$ is usually equal to 1.

To determine the equation of the curved surface, it is necessary to determine the control vertex $\boldsymbol{P}_{i,j}=[x_{i,j},y_{i,j},z_{i,j},1]$, i.e., to back-calculate a linear system of equations of the set of control vertex $\boldsymbol{p}_{i,j}$ (i=0, 1, … , r+k–1; j=0, 1, … , s+l–1) from the given set of data point $\boldsymbol{Q}_{i,j}$ (i=0, 1, … , r; j=0, 1, … , s). However, the set of linear equations for the curved surface is too large, which brings difficulties in solving the results and computerization. The back calculation problem of the curved surface is generally decomposed into the back calculation problems of the quadratic NURBS curved surface in the ***u***- and ***v***-directions, respectively.

The specific determination method is as follows:

$$\boldsymbol{a}_i(v)=\sum_{j=0}^{n}\boldsymbol{P}_{i,j}N_{j,l}(v_j) \tag{18}$$

where $\boldsymbol{a}_i(v)$ is a NURBS curved surface in the ***v***-direction. Eq.(17) can be rewritten as an expression similar to the equation of a non-uniform rational B-spline curve:

$$\boldsymbol{S}(u,v)=\sum_{i=0}^{m}N_{i,k}(u)\boldsymbol{a}_i(v_j) \tag{19}$$

As a result, the back calculation of the B-spline curved surface can be divided into the back calculations of the curved surface in two directions according to the abovementioned process. First, in the ***u***-direction, the non-uniform rational B-spline basis functions on the node vector and the set of data point $\boldsymbol{Q}_{i,j}$ (i.e., let $\boldsymbol{Q}_{i,j}=\boldsymbol{S}(u,v)$) are substituted into Eq.(19) to obtain m+1 point $\boldsymbol{a}_i(v_j)$ (i=0, 1, … , m; j=0, 1, … , n) on the control curve in the ***v***-direction. Then control vertex $\boldsymbol{p}_{i,j}$ can be obtained by substituting these points into Eq.(18) as the set of data points. Similarly, the B-spline basis function on the node vector $\boldsymbol{V}$ can be obtained by applying the same formula as the B-spline basis function on the node vector $\boldsymbol{U}$, and the control vertices corresponding to the data points in both directions of the NURBS curved surface can be inversely calculated.

The system of equations is represented by the matrix $\boldsymbol{Q}=\boldsymbol{BP}$. We can deduce $\boldsymbol{P}=\boldsymbol{B}^{-1}\boldsymbol{Q}$, where

$$\boldsymbol{B}=\begin{bmatrix}
\frac{3}{t_1-t_2} & \frac{3}{t_1-t_0} & 0 & & 0 & 0 & 0\\
N_{3,4}(t_0) & N_{-2,4}(t_0) & N_{-1,4}(t_0) & \cdots & 0 & 0 & 0\\
0 & N_{-2,4}(t_1) & N_{-1,4}(t_1) & & 0 & 0 & 0\\
 & \vdots & & \ddots & & \vdots & \\
0 & 0 & 0 & & N_{n-2,4}(t_0) & N_{n-2,4}(t_0) & 0\\
0 & 0 & 0 & \cdots & N_{n-1,4}(t_0) & N_{n-1,4}(t_0) & N_{n-1,4}(t_0)\\
0 & 0 & 0 & \cdots & 0 & \frac{3}{t_{n+1}-t_n} & \frac{3}{t_{n+1}-t_n}
\end{bmatrix} \tag{20}$$

where $N_{i,k}(t)$ is the ith k-order B-spline basis function, and $t(t_0,\ t_1,\ t_2,\ t_{n+1})$ is the node value.

2.2.2 Calculation of structural plane intersection lines and block vertices

Suppose that the coordinates of the centers of two structural planes are $O_1(x_1,y_1,z_1)$ and $O_2(x_2,y_2,z_2)$, and the radii are R_1 and R_2, and the normal vectors are (l_1,m_1,n_1) and (l_2,m_2,n_2), respectively. If the two structural planes have an intersection line, then the direction vector of the intersection line is $\boldsymbol{s}=(m_1n_2-n_1m_2,\ n_1l_2-l_1n_2,\ l_1m_2-m_1l_2)$. The coordinate of a point on the intersection line is denoted as $M(x_m,y_m,z_m)$. If there exists solutions for the following equation shows, the two structural planes have an intersection line. The two structural planes do not have an intersection line, if there exists no solution for the following equation shows:

$$\left.\begin{aligned}
&l_1(x_{\mathrm{m}}-x_1)+m_1(y_{\mathrm{m}}-y_1)+n_1(z_{\mathrm{m}}-z_1)=0\\
&l_2(x_{\mathrm{m}}-x_2)+m_2(y_{\mathrm{m}}-y_2)+n_2(z_{\mathrm{m}}-z_2)=0\\
&\frac{\left|\overrightarrow{O_1M}\times\boldsymbol{s}\right|}{|\boldsymbol{s}|}\leqslant R_1\\
&\frac{\left|\overrightarrow{O_2M}\times\boldsymbol{s}\right|}{|\boldsymbol{s}|}\leqslant R_2
\end{aligned}\right\} \tag{21}$$

Suppose that the plane equations of three structural planes are $A_ix+B_iy+C_iz+D_i=0$, $A_jx+B_jy+C_jz+D_j=0$, and $A_kx+B_ky+C_kz+D_k=0$, and the radii are R_1, R_2, and R_3, respectively. If the three structural planes have intersection points, the coordinates of the intersection points can be calculated as follows:

$$\left.\begin{aligned} &A_i x + B_i y + C_i z + D_i = 0 \\ &A_j x + B_j y + C_j z + D_j = 0 \\ &A_k x + B_k y + C_k z + D_k = 0 \\ &(x - x_1)^2 + (y - y_1)^2 + (z - z_1)^2 \leqslant R_1^2 \\ &(x - x_2)^2 + (y - y_2)^2 + (z - z_2)^2 \leqslant R_2^2 \\ &(x - x_3)^2 + (y - y_3)^2 + (z - z_3)^2 \leqslant R_3^2 \end{aligned}\right\} \quad (22)$$

After obtaining the coordinates of the intersection points of the structural planes, it is necessary to judge whether the intersection points are inside the rock slope. If the z-axis coordinate of the intersection point is smaller than the z-axis coordinate of the point on the rock slope with the same x-axis and y-axis coordinates, the intersection point is inside the rock slope.

2.2.3 Formation of closed loops on the free faces

Many blocks will be formed after rock masses being cut by structural planes, but only the stability of a few movable finite blocks need to be analyzed. The primary condition for a movable block is that there are closed outcropping traces on the free faces.

Whether a closed loop is formed on the free face can be determined by the following processes: (a) Calculate the intersection line between a structural plane and other structural planes. (b) If there are more than one intersection points between this structural plane and other structural planes (otherwise this structural plane can be regarded as an invalid structural plane), these intersection points are then projected onto the *XOY* plane. An invalid structural plane is shown in Fig. 3(a). (c) Calculate the intersection points between line segments on the *XOY* plane. (d) Search and delete the line segments with the number of nodes less than 2. (e) Until it is impossible to delete line segments, these structural planes can form loops with 3 or more nodes retained, as shown in Fig. 3(b).

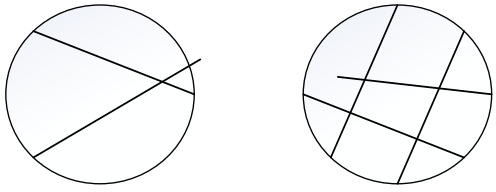

(a) Invalid structural plane (b) Valid structural plane

Fig. 3 Identification diagram of closed blocks

Figure 4(a) shows the structural plane before the loop search. Once the structural plane on the free face is closed, Fig. 4(b) shows the exposed plane of the block unit formed on the free face after the structural plane screening.

After getting the numbers of faces, edges, and vertices of blocks, we can use Euler's theorem of polyhedra to determine whether they constitute blocks. Euler's theorem for polyhedra: for a simple polyhedron, there is a famous Euler formula D–E+F=2 between the number of vertices D, the number of edges E, and the number of faces F. Through continuous deformation of the surface, a simple polyhedron can be transformed into a curved surface polyhedron.

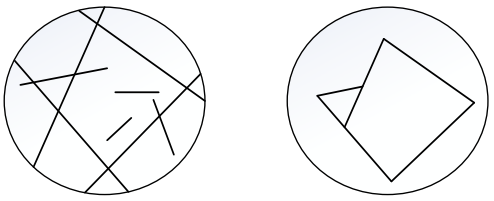

(a) Before loop search (b) After loop search

Fig. 4 Search graph of closed blocks

2.2.4 Block geometry analysis

Once being found, the closed blocks on the free face are geometrically analyzed to determine whether it is unstable, and to obtain its volume and structural plane area.

2.2.4.1 Determination of blocks with down-dip sliding surface

Geometric analysis requires the identification of the sliding surface of blocks. The most common blocks in the rock slope are blocks with a single sliding surface and double sliding surfaces. It is widely accepted that the block with an anti-dip sliding surface is stable and is not conducive to sliding. Hence, therein only the block with the down-dip sliding surface is discussed.

The sliding direction of the closed block with the down-dip sliding surface on the free face is denoted as the vector $\boldsymbol{S}$. $\boldsymbol{S}$ must satisfy the following equation:

$$\boldsymbol{n}_i \cdot \boldsymbol{S} \geqslant 0, (i = 1, \cdots, N) \quad (23)$$

where $\boldsymbol{n}_i$ is the inward unit normal vector of the block boundary surface.

The physical meaning of Eq.(23) is that all block surfaces will not resist the block sliding. Fig. 5(a) shows the projection of the block with single sliding surface. If the inner product of the normal vector and the sliding vector of the two structural planes is equal to or larger than zero, the sliding of the block will not be constrained, and this block is the potentially unstable block. In contrast, in Fig. 5(b), the angle between the normal vector and the sliding vector on the third structural plane is obtuse, which prevents the block from moving along this direction. Thus, the block can be considered stable.

2.2.4.2 Determination of structural plane area and volume of block

Based on the orthographic projection principle, the area of the structural plane can be obtained by the area

projection method combined with the dip angle of the structural plane. If the surface area of the structural plane and the dip angle of a block is S and β respectively, then the surface area of the structural plane can be expressed by the projected area on the (XOY) horizontal plane as follows:

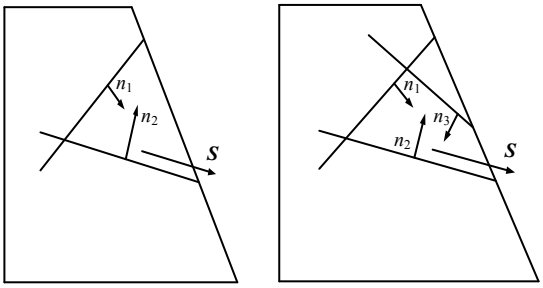

(a) Movable block (b) Immovable block

Fig. 5 Block slide diagram

$$S = S_{\mathrm{H}} / \cos\beta \tag{24}$$

Similarly, if the structural plane of the block is upright but not perpendicular to the XOZ and YOZ planes, the area of the structural plane can be obtained by the projections on the XOZ and YOZ planes.

The area of the structural plane projected on the horizontal plane S_{H} can be calculated as follows:

As the pentagonal projection shown in Fig. 6, the boundary nodes are sorted in clockwise order as A_1, A_2, A_3, A_4, A_5, with the origin $O(0,0,0)$, and the area of the polygon $A_1A_2A_3A_4A_5$ can be expressed as the area of $OA_1A_2A_3A_4$ minus the area of $OA_1A_5A_4$. Since the vector product of two vectors is two times the area of the triangle enclosed by the two vectors, the area of the pentagon can be obtained as

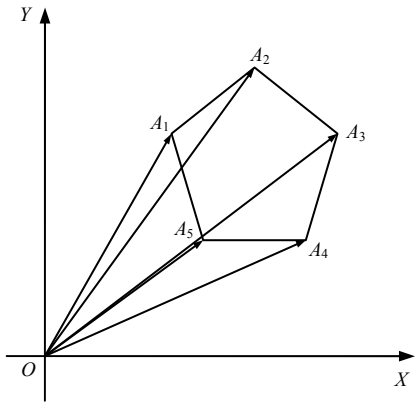

Fig. 6 Horizontal projection of a structural plane

$$S_{\mathrm{H}} = \frac{1}{2}\times \left|(\vec{OA_1}\times\vec{OA_2}+\vec{OA_2}\times\vec{OA_3}+\vec{OA_3}\times\vec{OA_4}-\vec{OA_1}\times\vec{OA_5}-\vec{OA_5}\times\vec{OA_4})\right| \tag{25}$$

Since the free face of the curved surface block may be an irregular curved surface, some line segments in the polygon may be curved. Therefore, the area S of the curved surface can be solved after dividing the surface into small areas.

As shown in Fig. 7(a), the area of the block surface can be obtained based on Eqs.(24) and (25). The slice method can be used to solve the volumes of plane and curved surface blocks. The slice method is an approximate method of dividing the block into many slices by a set of imaginary auxiliary planes parallel to a projection plane and solving the volume of each slice, as shown in Fig. 7(b). Then the volume of the block can be regarded as the sum of the volumes of the slices. Computer programming is easily completed for this method.

The block is cut with e rows of planes R_1, R_2, …, R_e to obtain e+1 slices (denoted as 1, 2, ... , e+1, respectively). Suppose the spacings of the adjacent two slices are l_2, … , l_e, respectively, and the areas of the slices are denoted as S_1, S_2, ... , S_e, and the slices 1 and e+1 are pyramids, and the slices 2, 3, ... , e are prisms, respectively, then the volume of the block can be calculated as:

$$V = \frac{1}{3}(S_1\cdot l_1 + S_e\cdot l_{e+1}) + \frac{1}{3}\sum_{i=2}^{e} l_i(S_{i-1}+S_i+\sqrt{S_{i-1}\cdot S_i}) \tag{26}$$

If the slice is thin, the top and bottom surfaces of the angular truncated cone are approximately expressed by their average values, Eq.(26) can be simplified as:

$$V = \frac{1}{3}(S_1\cdot l_1 + S_e\cdot l_{e+1}) + \frac{1}{2}\sum_{i=2}^{e} l_i(S_{i-1}+S_i) \tag{27}$$

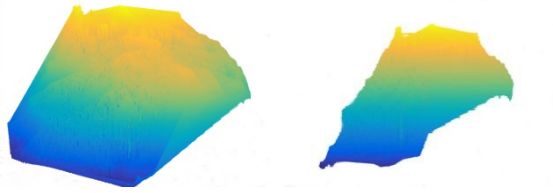

(a) Block geometry (b) Block cut by the horizontal plane

Fig. 7 Block profile

2.3 Stability calculation method of rocky slope blocks

The most common slope blocks are blocks with single sliding surface and double sliding surfaces. When analyzing the block stability by the coordinate projection method, the analytical method must be involved. For the unstable block with single sliding surface exposed on the rocky slope, the block slides along the sliding surface, i.e., the sliding direction points to the true dip angle of the sliding surface. At this time, if the block slides, its stability coefficient η can be determined by the following formula:

$$\eta = \frac{N\tan\varphi + cS_{\mathrm{f}}}{G\sin\beta} = \frac{G\cos\beta\tan\varphi + cS_{\mathrm{f}}}{G\sin\beta} \quad (28)$$

where G is the weight of the block; β is the dip angle of the sliding surface; S_{f} is the area of the sliding surface; and c and φ are the cohesion and friction angle of the sliding surface.

Blocks with double sliding surfaces are divided into planar and non-planar blocks, and tetrahedral blocks are the most common planar blocks. The stability coefficient η of the block is the ratio of the sum of the anti-slide forces available from the block on the projection axis to the sum of the forces causing the block to break on the projection axis:

$$\eta = \frac{N_1\tan\varphi_1 + N_2\tan\varphi_2 + c_1S_{\mathrm{f1}} + c_2S_{\mathrm{f2}}}{G\sin\beta} \quad (29)$$

where N_1 and N_2 are respectively the normal decomposition forces of the block weight G along the two structural planes; β is the dip angle of the intersected prism of the sliding surfaces; φ_1 and φ_2 are the friction angles of the two structural planes; c_1 and c_2 are the cohesions of the two structural planes; and S_{f1} and S_{f2} are the areas of the two sliding surfaces.

According to the classification standard of the stability degree of dangerous rock masses in the *Specification of geological investigation for landslide stabilization* (DZ/T 0218−2006)[34], the blocks are unstable for the stability coefficient of dangerous rock masses forming landslides $\eta < 1.0$, potentially unstable for $1.0 \leqslant \eta < 1.2$, basically stable for $1.2 \leqslant \eta < 1.3$, and stable for $1.3 \leqslant \eta$.

3 Visualization of block stability analysis

Since the coordinate projection mapping of blocks, especially multi-blocks, is complex and inefficient, it is necessary to conduct computerization and visualization of the mapping. In this paper, based on the coordinate projection method, the CPG program is developed by using the development environment and graphics processing toolbox of MATLAB[35−36] and UAV technology used to acquire data. The program can be used to easily determine the block geometry conditions and to realize the stability analysis and visualization of the block, and it can be applied to engineering practices with high efficiency.

3.1 Data acquisition by UAV technology and data processing

Before the stability analysis of the rocky slope block, the images of the concerned areas of the slope need to be collected as basic data. In this paper, the UAV technology is used for data acquisition, and the real scene 3D modelling software Context Capture is used to process the images and generate colored point clouds, which are finally transformed into 3D coordinates used by the coordinate projection method. Those specific procedures are as shown in Fig. 8.

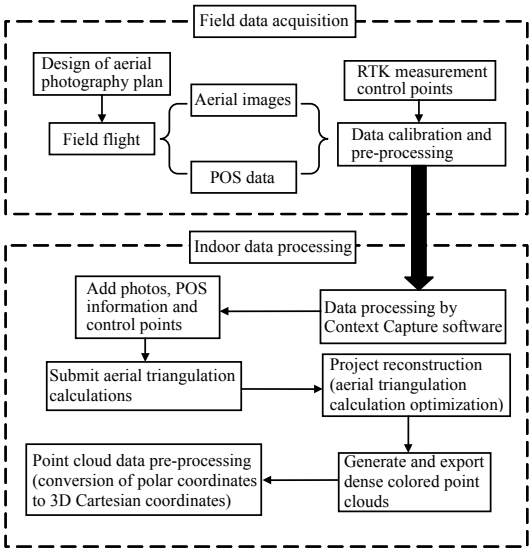

Fig. 8 Data collection and processing flow chart

3.1.1 Field data acquisition by UAV

A Dajiang Phantom 4 quadcopter UAV with fixed-wings was used for the survey. Due to the complex terrain, steep cliffs in topography, and the nearly upright slope with the aspect of 278° around the concerned area, the upright flight up and down of the UAV taking full advantage of its small size was chosen to ensure the flight safety and the accurate and complete slope information collection. According to the *Specification for low-altitude digital aerial photography* (CH/Z 3005−2010)[37], the overlap rates of the heading and side directions were both set to 70%, and the relative flight height was set to 150 m. The layout of the UAV route and the scope of the survey area are shown in Fig. 9. To ensure the high quality of the aerial images, the image resolution was set to 4.1 cm. The typical images captured by the UAV aerial photography are shown in Fig. 10.

Parameters such as longitude, latitude, flight altitude, and flight attitude of each photo were extracted and filtered from the flight controller to form a complete POS (position orientation system) information. Then several obvious locations were selected as control points, and their position and elevation information were measured and recorded by GPS (global positioning system) and RTK (real time kinematic) to correct the corresponding position and elevation information of the generated point cloud data. A total of 6 image control points and 5 check points were evenly distributed

in the aerial photography area. A total of 122 355 aerial triangulation connection points were solved, and the mean square error of the calculated residuals was 0.018 m.

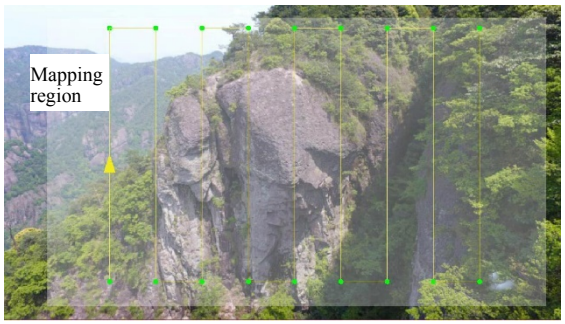

Fig. 9 UAV route map

Fig. 10 UAV aerial image

3.1.2 Indoor data processing of UAV

The images scanned by the UAV need to be processed by the real scene 3D modeling software Context Capture to obtain the point cloud data. The specific steps include:

(1) Data import. Add aerial images and POS information files containing latitude, longitude, elevation, and flight attitude to Context Capture.

(2) Set downsampling and examine the image files. Downsampling can reduce the amount of information to be processed, and thus the 3D model draft can be quickly generated to create sparse point clouds.

(3) Place control points. Adding control points can correct the POS information, and the aerial triangulation calculation becomes more accurate by adjustment according to the control points.

(4) Optimize the camera alignment parameters. After puncturing the control points, the sensor size and focal length of camera lens are optimized to make the calculation results more accurate and to avoid distortions.

(5) Submit aerial triangulation for "Reconstruction" if needed. A reference 3D model and colored point clouds are generated to perform the visualization and analysis in the CPG program.

The data obtained from the UAV aerial photography cannot be used directly before being pre-processed[38]. The data need to be stitched together firstly before being processed. The data of each scan are independent of each other, and the spatial coordinate systems of the data are different, but they all use the center of the UAV as the coordinate origin. The discrete coordinate systems can be transformed into a single coordinate system by the coordinate conversion.

The data obtained from the UAV aerial photography is in the spatial polar coordinate format. The spatial polar coordinate of a point P is denoted by (σ, ε, δ). The Cartesian coordinate system is established with the UAV as the origin, and the Cartesian coordinate of the point P is denoted as (x, y, z). Now the polar coordinates can be converted to Cartesian coordinates. As shown in Fig. 11, O is the coordinate origin, P is the target point to be measured, and the Cartesian coordinate of point P can be expressed in polar coordinates as

$$\left.\begin{aligned} x &= \sigma \sin\delta \sin\varepsilon \\ y &= \sigma \sin\delta \cos\varepsilon \\ z &= \sigma \cos\delta \end{aligned}\right\} \quad (30)$$

where σ is the distance from the point P in polar coordinates to the origin O; ε is the azimuthal angle between the coordinate plane ZOY and the half-plane through the Z-axis and the point P; and δ is the elevation angle between the line segment OP and the positive direction of the Z-axis.

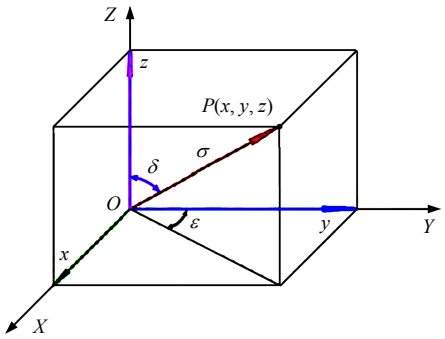

Fig. 11 Coordinate transformation diagram

After the above conversion, the polar coordinate data acquired by the UAV have been converted to the Cartesian coordinate data that can be applied in the coordinate projection method, as listed in Table 1.

3.2 Block stability analysis program—CPG

The CPG program is developed based on MATLAB and the coordinate projection method. The program is feasible owing to the human-computer interface, and greatly simplifies the development steps of the operation interface. It uses the image processing toolbox to display images, which can truly show the 3D slope model and the position of unstable blocks. Moreover, it has some functions such as data input and output, and visualization of model rotation, translation and scaling.

Table 1 Slope point cloud data

Order of point cloud (Partly)	*x*-coordinate	*y*-coordinate	*z*-coordinate	RGB color information		
				Red	Green	Blue
1	3.771	10.034	0.551	211	195	204
2	7.464	0.873	−0.217	111	113	135
3	4.646	9.421	−5.083	137	129	148
4	8.462	4.781	1.915	133	114	120
5	7.489	0.897	−0.203	102	104	125
6	4.622	9.538	−5.164	136	127	140
7	7.494	0.899	−0.313	112	115	136
8	7.484	0.759	−0.219	112	115	139
9	8.366	4.908	1.818	116	98	106
10	7.489	0.954	−0.258	125	126	146
11	4.658	9.427	−5.175	192	182	199
12	7.483	0.874	−0.331	99	102	124
13	8.420	4.790	1.823	141	122	132
14	7.499	0.842	−0.258	141	143	166
15	7.494	0.786	−0.202	118	120	144
16	7.485	0.760	−0.333	96	99	124
17	7.496	0.860	−0.292	128	131	153
18	7.493	0.953	−0.204	155	156	177

The CPG program has the following 5 functions:

(1) CPG-I program

The main function of the CPG-Ⅰ program is to import the pre-processed point cloud data that is further used to build a 3D visualization model of the rocky slope.

(2) CPG-II program

The CPG-II program is divided into two subprograms, i.e., CPG-II-1 and CPG-II-2. The CPG-II-1 program automatically searches for structural planes from the 3D model using an improved region growing algorithm; the CPG-II-2 program uses the human-computer interaction to calculate the structural plane equations by selecting point data from the model to supplement the structural planes that cannot be identified by the CPG-II-1 program. The output result is a spatial representation of the structural plane, where the data in the first column are constant terms, the data in the second column are the coefficients of the plane equation *x*, and the data in the third column are the coefficients of the plane equation *y* (the coefficient of the plane equation *z* is equal to 1).

(3) CPG-III program

The CPG-Ⅲ program can fit the free face equations with the plane data obtained from the UAV aerial photography using the NURBS method. The blocks partitioned by the structural plane and the free face are quantitatively analyzed and the potentially unstable closed blocks are identified in the program. The output data are divided into two parts: the control points of the free face and the information of the potentially unstable blocks. The first column of the block information is the block number. In the second column, "1" represents that the block is closed, while "0" represents that the block is open. The last three columns are the numbers of the structural planes constituting the block.

(4) CPG-IV program

The CPG-IV program is mainly used for geometric analysis of the closed blocks identified by the CPG-III. Firstly, it determines whether the closed block is unstable, and then the potentially unstable blocks are selected to calculate the areas of boundary surfaces and the entire volume. The meanings of the output data are: the first column indicates the number of the first selected structural plane, and the second column indicates the area of the first structural plane, and so on. The last column represents the volume of the block partitioned by the above structural planes.

(5) CPG-V program

Based on the information of potentially unstable blocks obtained by the CPG-IV program, the block parameters are input in the CPG-V program interface to calculate the stability coefficient, and unstable blocks are thus determined and visualized.

4 Engineering applications

To verify the reliability of the CPG program, the stability analysis of the Shenxianju slope blocks in Zhejiang Province was carried out using the CPG program.

4.1 Project overview

Shenxianju in Xianju County, Zhejiang Province, the largest typical volcanic rhyolite landform in the world, is a national 5A-level scenic spot with a total area of 22.32 km^2. It is located between the low hill area of eastern Zhejiang and the middle mountain area of southern Zhejiang, with an altitude of 100−900 m and a relative height difference of 200−600 m. The terrain in the scenic spot is strongly cut, with a maximum cutting depth of 800 m. The slope changes sharply, and the upper part of the mountain is flat, while the central part has many cliffs with steep terrain and abrupt mountains. The block instability and collapse occur frequently there.

The physical and mechanical parameters of the rocks on the high and steep rocky slope in Shenxianju are listed in Tables 2 and 3.

Table 2 Basic physical indicators of Shenxianju slope rock

Test items	Natural density ρ/(g • cm^{-3})	Dry density ρ_d/(g • cm^{-3})	Saturation density ρ_w/(g • cm^{-3})	Natural water content w /%
Average value	2.57	2.21	2.31	4.31

Table 3 Basic mechanical properties of Shenxianju slope rock

Water content of the specimen	Elastic modulus /GPa	Poisson's ratio	Uniaxial compressive strength /MPa	Cohesion /MPa	Internal friction angle /(°)	Tensile strength /MPa
Air seasoning	13.36	0.166	203.46	20.32	76	6.58

4.2 Analysis of results

4.2.1 3D slope model

The processed point cloud data of the slope in section 3.1 (Table 1) were input into the CPG-I program to establish the 3D slope model. Then the visualized real scene view of the rocky slope in Fig. 12(a) and the 3D spatial model of the rocky slope in Fig. 12(b) could be obtained.

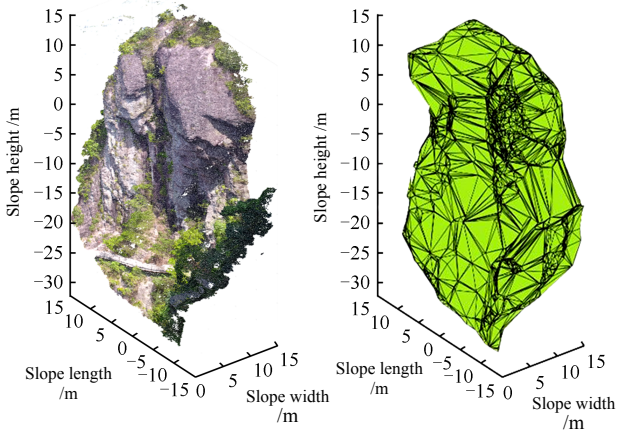

(a) Visualization figure (b) Modelling diagram

Fig. 12 3D model and visualization of the slope

4.2.2 Determination of the structural plane

Based on the established 3D slope model, the structural planes in the rock mass were identified by the CPG-II program. Firstly, clicked "Automatic identification of structural planes" in the main interface of the CPG program, i.e., ran CPG-II-1 program to obtain the point cloud of the structural plane. Deleted the point cloud group with few units since there were extensive UAV data points. Then added the unselected structural plane through the CPG-II-2 program, as shown in Fig. 13, and the coefficients of 19 structural plane equations were obtained, as listed in Table 4.

Taking the three points on the No. 3 structural plane constituting the No. 1 block that were not in the same line as an example, A (8.366, 4.908, 1.818), B (7.489, 0.954, 0.258), and C (4.658, 9.427, 5.175), the structural plane equations $\hat{\theta}_0, \hat{\theta}_1, \hat{\theta}_2$ were calculated manually. The structural surface equation coefficients could then be obtained by Eq.(6), which was the same as the No. 3 structural plane coefficients in Table 4. The expression is $\hat{z}_3$=2.513 1x_3+ 5.332 5y_3−48.873 2. Similarly, the equation coefficients of No. 5 and No. 8 structural planes were calculated and combined with Eqs.(7) and (8) to obtain their occurrences, and the results are listed in Table 5.

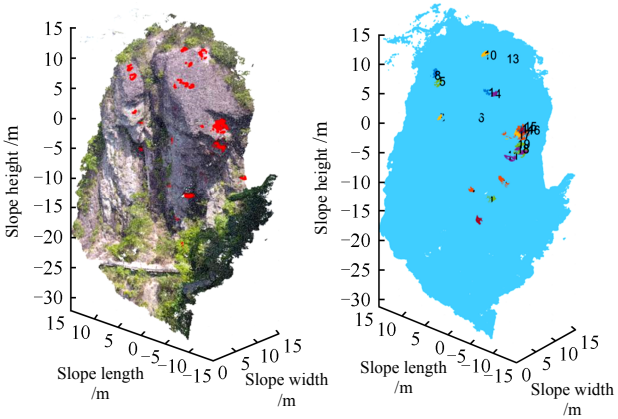

(a) Point cloud map of the structural plane (b) Number of the structural plane

Fig. 13 Point cloud map and number of the structural plane

Table 4 Equation coefficient of the structural plane

Structural plane number	Equation coefficient of the structural plane	Structural plane number	Equation coefficient of the structural plane
1	−1.990 3, 1.687 5, 1.074 5	11	13.235 6, −1.970 6, −0.831 2
2	62.493 3, −7.586 8, −3.676 0	12	−22.193 9, 1.253 1, 3.166 3
3	−48.873 2, 2.513 1, 5.332 5	13	8.094 7, 0.470 5, 0.503 1
4	−7.567 0, 3.113 6, 3.125 4	14	2.282 5, 1.687 2, 3.010 6
5	−29.918 1, 2.587 4, 3.424 3	15	3.714 5, 1.547 0, 2.990 6
6	20.063 0, −2.517 4, −1.228 4	16	3.938 8, 1.825 8, 3.513 4
7	−47.250 5, 3.516 6, 0.494 3	17	1.388 0, −0.402 0, −0.669 0
8	−6.176 8, 0.774 4, 1.444 2	18	10.435 7, 4.404 3, 10.773 6
9	29.552 1, −3.738 5, −0.954 1	19	14.979 3, 8.257 3, 19.073 4
10	5.477 5, 0.689 4, 0.155 7	—	—

Table 5 Occurrence of structural planes 3, 5 and 8

Structural plane number	Strike /(°)	Dip direction	Dip angle /(°)
3	27	NE	80
5	142	SW	77
8	115	SE	59

4.2.3 Determination of block volume and structural plane area

The output results of the CPG-I and CPG-II programs were input to the CPG-III program to obtain: (a) the control points of the free face equations (Table 6) and the corresponding equations by substituting the control points into Eq.(16); (b) information of potentially unstable blocks (Table 7).

The volume of the closed block and the area of each structural plane obtained by CPG-III were calculated by the CPG-IV program (Table 8).

Table 6 Surface control points

Number of the control point	Control point of the curved surface	Number of the control point	Control point of the curved surface
1	1.910 0, 14.019 0, −13.063 0	12	12.100 0, −4.887 0, 8.726 0
2	7.035 0, 6.854 0, −3.135 0	13	11.142 0, −4.779 0, 8.152 0
3	8.407 0, −4.417 0, −1.918 0	14	10.414 0, 3.609 0, 11.492 0
4	3.884 0, 10.489 0, 2.388 0	15	9.160 0, 3.176 0, 10.277 0
5	4.452 0, 13.618 0, −6.443 0	16	8.648 0, 4.581 0, 1.965 0
6	1.506 0, 10.509 0, −21.180 0	17	14.161, −13.228 0, −13.194 0
7	1.472 0, −3.462 0, −27.197 0	18	6.798 0, −14.305 0, −15.574 0
8	1.455 0, 12.476 0, −18.703 0	19	9.619 0, −13.033 0, −14.608 0
9	1.098 0, 6.372 0, −22.889 0	20	11.539 0, −10.151 0, −14.923
10	1.176 0, 2.356 0, −26.217 0	21	12.181 0, −8.121 0, −13.972 0
11	12.338 0, −2.332 0, 11.624 0	—	—

Table 7 Information of potentially unstable blocks

Block number	Closed state	Structural plane number
1	1	3，5，8
2	1	10，13，14
3	1	14，15，17
4	1	14，16，19
5	1	11，18，19
6	0	1，3，7
7	0	13，14，15
8	0	6，8，13
9	0	7，14，16

The equations of structural No. 3, 5, and 8 planes were calculated manually and combined with Eq.(22) to calculate the coordinates of the block vertices, which could be further used to obtain the structural plane areas S_3 =6.864 6 m^2, S_5 =5.456 2 m^2, S_8 = 8.435 4 m^2 and the block volume V_1=4.722 3 m^3. The results are the same as those obtained by the program calculation.

4.2.4 Block stability analysis

The stability coefficients of the blocks were calculated by inputting the weight γ, Poisson's ratio μ, cohesion c, and internal friction angle φ of the blocks in the CPG-V program, and the results are listed in Table 8. The locations of these blocks were also displayed in the slope, as shown in Fig. 14.

The calculation results show that the stability coefficient of the No. 4 block is 0.918 8 (<1), which can be regarded as an unstable block; the stability coefficient of No. 3 block is 1.193 9, which can be regarded as a potentially unstable block. Engineering practice shows that the No. 4 block fell in April 2017 without causing casualties, and the No. 3 block has not fallen yet but needs to be reinforced and supported accordingly.

Table 8 Comparison among the block stability coefficients

Block number	Structural plane number	Structural plane area /m^2	Block volume /m^3	Stability coefficient (calculated by the CPG program)	Stability coefficient (Manual calculation)	Stability state (CPG program)
1	3，5，8	6.864 6, 5.456 2, 8.435 4	4.722 3	1.365 8	1.357 7	Stable
2	10，13，14	3.645 1, 9.185 6, 5.843 2	4.678 5	1.297 4	1.165 9	Basically unstable
3	14，15，17	8.261 4, 10.772 8, 3.852 7	3.528 2	1.193 9	1.063 5	Potentially unstable
4	14，16，19	2.582 1, 12.726 9, 4.283 4	7.659 1	0.911 8	0.828 3	Unstable
5	11，18，19	6.468 4, 7.465 3, 4.953 0	3.786 8	1.853 3	1.718 1	Stable

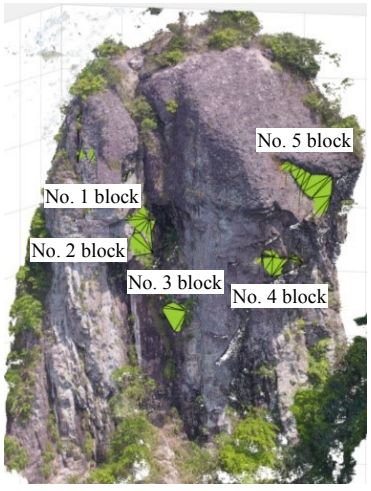

Fig. 14 Diagram of potential unstable blocks

4.2.5 Comparison between the stability coefficients by the CPG program and manual calculation

To verify the reliability of the results of the engineering project calculated by the program, the dip angle β, area S of the structural planes, and block volume V of Nos. 1−5 blocks were calculated manually. The stability coefficient of each block was calculated by Eq.(29) combining the parameters in Tables 2 and 3: η_1=1.357 7, η_2=1.165 9, η_3=1.063 5, η_4=0.828 3, η_5=1.718 1.

The stability coefficients calculated by the CPG program were compared with those by manual calculation, and the results are basically consistent, as shown in Table 8. The Pearson correlation coefficient of the CPG and manual calculations is 0.987, indicating that the correlation is significant. This indicates that the engineering analysis results by the program calculation are reliable.

5 Conclusions

(1) The 3D point cloud data of the rock slope were

obtained by UAV aerial photography, and the 3D visualization model of the slope was established, which improved the efficiency and safety.

(2) Based on the coordinate projection method, we proposed to fit the equations of the structural plane by the linear regression method and the equations of the free face by the non-uniform rational B-spline method. Then the topology search and vector analysis were combined to quantitatively analyze the blocks cut by the structural plane and the free face to obtain finite closed blocks. Based on the geometric information of the blocks, the potentially unstable blocks were identified and their stability coefficients were calculated. The unstable blocks in the rocky slope were finally identified and their specific locations were displayed in the 3D model.

(3) Using the CPG program, the 3D model of the rocky slope was established by importing point cloud data. Then the structural plane and free face were fitted, and potentially unstable blocks and unstable blocks were identified. Finally, the stability analysis and visualization of blocks were carried out.

(4) According to the correlation analysis, the results of engineering practice calculated by the CPG program and the coordinate projection method are basically consistent, indicating that the analysis results are reliable.

Reference

[1] WANG Si-jing, YANG Zhi-fa, LIU Zhu-hua. Stability analysis of rock mass in underground engineering[M]. Beijing: Science Press, 1984.

[2] YANG Zhi-fa, WANG Si-jing, GAO Bing-li. Coordinate projection mapping method and its application in rock block stability analysis[M]. Beijing: Science Press, 2009.

[3] GOODMAN R E, SHI G H. Block theory and its application to rock engineering[M]. [S. l.]: Prentice Hall, 1985.

[4] SUN Yu-ke, GU Xun. Application of the stereographic projection in engineering geomechanics of rock masses[M]. Beijing: Science Press, 1980.

[5] SHI Gen-hua. Stereographic projection method for rock mass stability analysis[J]. Science China, 1977(3): 260−271.

[6] LIN D, FAIRHURST C, STARFIELD A M. Geometrical identification of three-dimensional rock block systems using topological techniques[J]. International Journal of Rock Mechanics and Mining Sciences & Geomechanics Abstracts, 1987, 24(6): 331−338.

[7] DU Song, XIAO Ming, CHEN Jun-tao. Study on catastrophe progression method for geological block hazard analysis of underground caverns[J]. Rock and Soil Mechanics, 2021, 42(9): 2578−2588.

[8] YOSSEF H，HATZOR M. Key block stability in seismically active rock slopes—snake path cliff, Masada[J]. Journal of Geotechnical & Geoenvironmental Engineering, 2003, 129(8): 697−710.

[9] CHEN Hu, YE Yi-cheng, WANG Qi-hu, et al. Study of direct roof failure form of soft layer in roadway based on rock beam-block theory[J]. Rock and Soil Mechanics, 2020, 41(4): 1447−1454.

[10] JIANG Shui-hua, OUYANG Su, FENG Ze-wen, et al. Reliability analysis of jointed rock slopes using updated probability distributions of structural planes parameters[J]. Rock and Soil Mechanics, 2021, 42(9): 2589−2599.

[11] DING Wen-qi, ZHENG Kang-cheng, LI Xiao-ran, et al. The calculation method of three-dimensional shear strength of rock structural plane based on 3D printing technology[J]. Rock and Soil Mechanics, 2020(Suppl. 2): 1−9.

[12] LIU T X, DENG J H, ZHENG J, et al. A new semi-deterministic block theory method with digital photogrammetry for stability analysis of a high rock slope in China[J]. Engineering Geology, 2017, 216: 76−89.

[13] GUO J T, LIU S J, ZHANG P, et al. Towards semi-automatic rock mass discontinuity orientation and set analysis from 3D point clouds[J]. Computers and Geosciences, 2017, 103: 164−172.

[14] FRANCIONI M, SALVINI R, STEAD D, et al. Improvements in the integration of remote sensing and rock slope modelling[J]. Nat Hazards, 2018, 90(2): 975−1004.

[15] JIA Shu-guang, JIN Ai-bing, ZHAO Yi-qing. Application of UAV oblique photogrammetry in the field of geology survey at the high and steep slope[J]. Rock and Soil Mechanics, 2018, 39(3):1130−1136.

[16] WU Xu-dong. Development of software for visual analysis of rock mass stability based on block theory[D]. Nanjing: Hohai University, 2007.

[17] ZHOU Yang-yi, FENG Xia-ting, XU Ding-ping, et al. A simplified analysis method of block stability in large underground powerhouse[J]. Rock and Soil Mechanics, 2016, 37(8): 2391−2398.

[18] WANG S H, ZHANG Z S, WANG C G, et al. Multistep rocky slope stability analysis based on unmanned aerial vehicle photogrammetry[J]. Environmental Earth Sciences, 2019, 78(8): 260.

[19] ALBARELLI D S N, MAVROULI O C, NYKTAS P.

Identification of potential rockfall sources using UAV-derived point cloud[J]. Bulletin of Engineering Geology and the Environment, 2021, 80: 6539−6561.

[20] ZHANG L L, SHERIZADEH T, ZHANG Y W, et al. Stability analysis of three- dimensional rock blocks based on general block method[J]. Computers and Geotechnics, 2020, 124: 103621.

[21] JIN Ai-bing, CHEN Shuai-jun, ZHAO An-yu, et al. Numerical simulation of open-pit mine slope based on unmanned aerial vehicle photogrammetry[J]. Rock and Soil Mechanics, 2021, 42(1): 255−264.

[22] WANG S H, AHMED Z, HASHMI M Z, et al. Cliff face rock slope stability analysis based on unmanned arial vehicle (UAV) photogrammetry[J]. Geomechanics and Geophysics for Geo-Energy and Geo-Resources, 2019, 5(4): 333−344.

[23] LIU C, LIU X L, PENG X C, et al. Application of 3D-DDA integrated with unmanned aerial vehicle–laser scanner (UAV-LS) photogrammetry for stability analysis of a blocky rock mass slope[J]. Landslides, 2019, 16: 1645−1661.

[24] WANG F L, WANG S H, HASHMI M M Z, et al. The characterization of rock slope stability using key blocks within the framework of GeoSMA-3D[J]. Bulletin of Engineering Geology and the Environment, 2018, 77(4): 1405−1420.

[25] YANG Zhi-fa. Block coordinate projection mapping method and determination of block geometry[C]//Rock Mass Engineering Geomechanics (3). Beijing: Science Press, 1980: 171−202.

[26] GAO Bing-li. Computerization of coordinate projection mapping and its application in structural surface and block stability analysis[D]. Xi'an: Xi'an University of Science and Technology, 2005.

[27] GAO Bing-li, ZHANG Lu-qing, YANG Zhi-fa, et al. Computerization of coordinate projecting method and its application in geometry analyses of rock blocks[J]. Journal of Engineering Geology, 2005, 16(3): 376−381.

[28] YANG Zhi-fa, GAO Bing-li, ZHANG Lu-qing, et al. Computer description of structural planes and blocks based on coordination projection diagram and its application[J]. Chinese Journal of Rock Mechanics and Engineering, 2006, 25(12): 2392−2398.

[29] YUAN Guang-xiang, ZENG Qing-li, YANG Zhi-fa, et al. Application of coordinate projection mapping method in stability analysis of Suwaka rock slope in Sichuan-Tibet line[J]. Chinese Journal of Geological Hazard and Control, 2007, 18(3): 102−107.

[30] YUAN Guang-xiang, ZHANG Lu-qing, YANG Zhi-fa. Graphic method and its application in curved discontinuities[J]. Geotechnical Engineering Technology, 2009, 23(1): 5−8.

[31] SONG B, ZHENG N S, LI D W, et al. DEM reconstruction based on ground laser scanning point cloud data and NURBS surface[J]. Transactions of Nonferrous Metals Society of China, 2015, 25(9): 3165−3172.

[32] FAN Yi-yan. Research and development of free surface reconstruction based on NURBS[D]. Tianjin: Tianjin University, 2004.

[33] XU Guang-li, TANG Hui-ming, DU Shi-gui. Rock mass structure model and application[M]. Wuhan: China University of Geosciences Press, 1993.

[34] China Geological Survey. DZ/T 0218－2006 Specification of geological investigation for landslide stabilization[S]. Beijing, Standards Press of China, 2006.

[35] TANG Gao-peng, ZHAO Lian-heng, LI Liang, et al. Program development for slope stability using MATLAB software and upper bound limit analysis[J]. Rock and Soil Mechanics, 2013, 34(7): 2091−2098.

[36] XIE Li-hui. Slope stability analysis based on MATLAB optimization toolbox[J]. Shanxi Architecture, 2018, 44(14): 86−87.

[37] State Bureau of Surveying and Mapping. CH/Z 3005－2010 Specifications for low-altitude digital aerial photography[S]. Beijing: Surveying and Mapping Publishing House, 2010.

[38] LIU Jun-qiang, GAO Jian-min, LI Yan, et al. Research on cloud data's pretreatment technology based on reverse engineering[J]. Modern Manufacturing Engineering, 2005(7): 73−75.